The nuclear magnetic resonance line shapes of Xe in the cages of clathrate hydrates

Cynthia J. Jameson and Dirk Stueber
Department of Chemistry, M/C-111, University of Illinois at Chicago, Chicago, Illinois 60607-7061

(Received 20 November 2003; accepted 5 March 2004)

We report, for the first time, a prediction of the line shapes that would be observed in the ^{129}Xe nuclear magnetic resonance (NMR) spectrum of xenon in the cages of clathrate hydrates. We use the dimer tensor model to represent pairwise contributions to the intermolecular magnetic shielding tensor for Xe at a specific location in a clathrate cage. The individual tensor components from quantum mechanical calculations in clathrate hydrate structure I are represented by contributions from parallel and perpendicular tensor components of Xe–O and Xe–H dimers. Subsequently these dimer tensor components are used to reconstruct the full magnetic shielding tensor for Xe at an arbitrary location in a clathrate cage. The reconstructed tensors are employed in canonical Monte Carlo simulations to find the Xe shielding tensor component along a particular magnetic field direction. The shielding tensor component weighted according to the probability of finding a crystal fragment oriented along this direction in a polycrystalline sample leads to a predicted line shape. Using the same set of Xe–O and Xe–H shielding functions and the same Xe–O and Xe–H potential functions we calculate the Xe NMR spectra of Xe atom in 12 distinct cage types in clathrate hydrates structures I, II, H, and bromine hydrate. Agreement with experimental spectra in terms of the number of unique tensor components and their relative magnitudes is excellent. Agreement with absolute magnitudes of chemical shifts relative to free Xe atom is very good. We predict the Xe line shapes in two cages in which Xe has not yet been observed. © *2004 American Institute of Physics.*
[DOI: 10.1063/1.1718349]

INTRODUCTION

Clathrate hydrates are crystalline inclusion compounds consisting of a hydrogen-bonded network of polyhedral water cavities which encage small molecules. The cages are described by a notation M^n for n faces, each face having M sides; for example, $5^{12}6^2$ (12 pentagons and 2 hexagons). Natural deposits of predominantly methane hydrate are found in permafrost, in off-shore and on-shore sediments, the amount of gas estimated to be much larger than global combined fossil fuel reserves. It has been suggested that gas hydrates also exist in space, in some planets and their moons. Understanding the crystal structure, growth, and decomposition will have wide ranging implications in a variety of applications including efficient exploitation of gas reserves, in understanding the role of gas hydrates in space and in glaciology.[1] Furthermore, studies of clathrate hydrates contribute to a fundamental understanding of inclusion chemistry in general, particularly in hydrogen-bonded systems.

Xe nuclear magnetic resonance (NMR) spectroscopy has been a very useful tool for probing porous materials since the Xe atom, roughly the same size as a methane molecule, can explore confined spaces having dimensions that span those of interest in catalysis and separations. Furthermore, the isotropic intermolecular Xe chemical shift is exquisitely sensitive to environment. Thus, Xe chemical shifts have been used to characterize cavities in aluminosilicates, in molecular crystals, and in biological systems.[2–4] It has been demonstrated that even more detailed information is available in the Xe chemical shift tensor. Ripmeester and co-workers have discovered that experimental NMR line shapes of a single Xe guest atom in small cages exhibit either isotropic or anisotropic characteristics.[5–12] They have also observed anisotropic Xe line shapes in porous materials with nanochannels, and find that these lineshapes exhibit a systematic dependence on the Xe loading.[13–15] In the gas or liquid phase, Xe is free to explore all directions equally and one expects and observes isotropic lines in the ^{129}Xe NMR spectrum. In the highly anisotropic environments of nanopores and nanochannels where confinement precludes uniform averaging in all directions, one may expect to observe lineshapes that reflect the anisotropy of the environment. The anisotropy of the Xe chemical shift which can be obtained experimentally from the Xe NMR spectrum in the limit of zero occupancy should reflect the pore geometry, provided that the physical exchange of adsorbed Xe with the Xe atoms in the bulk phase is sufficiently slow. From such lineshapes the average Xe shielding tensor components may be extracted.

In general there are six distinct elements in the symmetric part of the shielding tensor. In order to be able to calculate all the Xe shielding tensor components for an arbitrary position of Xe within the cage, it will be necessary to represent the tensor components that are obtained quantum mechanically with interpolating functions which in turn may be used to provide tensor components for Xe at arbitrary locations. The shielding tensor of Xe in a particular configuration of water molecules is a complex function of the coordinates of all the oxygen and hydrogen atoms relative to the Xe atom. This is not a trivial task. Therefore, we make the as-

sumption that each of the Xe shielding tensor components (σ_{XX}, σ_{YY}, σ_{ZZ}, $(\sigma_{XY}+\sigma_{YX})/2$, $(\sigma_{XZ}+\sigma_{ZX})/2$, $(\sigma_{ZY}+\sigma_{YZ})/2$, in such a configuration in the laboratory frame, can be treated as a pairwise additive function of Xe–O and Xe–H shielding tensor components. The latter are assumed to depend on Xe–O and Xe–H distances in the same way that Xe tensor components $\sigma_{\parallel}$ and $\sigma_{\perp}$ of the Xe–Rg rare gas dimer depends on distance.[16] One of us has used this approach previously in the calculation of the Xe NMR line shapes in the nanochannels of ALPO-11.[17] This required the neglect of any many-body contributions to the intermolecular shielding tensor. There is experimental evidence of such deviations from pairwise additivity from the observations of neat liquid and gas phase NMR chemical shifts.[18–22] When all atoms involved are rare gas atoms, such as in $XeNe_n$ clusters or Xe_3 clusters, the many-body terms can be directly determined from the difference between the calculated shielding tensor components for the cluster and the pairwise sums of Xe–Ne or Xe–Xe shielding tensor components. A discussion of the many-body contributions and the deviations from pairwise additivity of the intermolecular shielding tensor is given elsewhere.[23] In this work we will neglect such many-body terms and assume pairwise additivity in the scheme known as the dimer tensor model, introduced by one of us.[17]

We have carried out nuclear magnetic shielding calculations for Xe in the cages of clathrate hydrate structures I and II.[24] In the previous paper, we discussed the various models explored in the attempt to represent, within practical limitations, the environment of a Xe atom trapped in a cage in a hydrogen-bonded network system. We showed that the electrostatic contributions to intermolecular shielding of a Xe atom are small and negligible, but the electrostatic contributions from neighboring water molecules in the extended lattice to the electronic structure of the water molecules of a cage are not negligible, and this has a corresponding effect on the Xe shielding response. When the hydrogen bonding of the water molecules of the cage is incompletely described (i.e., when their hydrogen-bonding partners are either absent or represented merely by partial point charges, thereby leaving out the covalent part of the hydrogen bonding), these molecules do not provide the correct shielding response at the Xe nucleus. By using five models that incorporate some but not all of the electronic coupling of the Xe atom to the water molecules in the crystal, we demonstrated which factors were important, and to what extent excluding them from the model compromises the description of Xe shielding in any hydrogen-bonded system. We provided a paradigm for the general treatment of intermolecular shielding in a hydrogen-bonded network. Universal Xe–O and Xe–H isotropic shielding functions were obtained by fitting together the quantum mechanical values calculated using several cages with diverse proton arrangements representing clathrate hydrate structure I. Simulation boxes consisting of supercells were used with the same set of isotropic shielding functions and the same set of potential parameters to provide Monte Carlo averages of the isotropic Xe shielding that were in good agreement with the values observed by Ripmeester *et al.* in the small and large cages of clathrate hydrate structures I and II.[5–7,11] The results presented there were the first calculations of the isotropic Xe shielding in clathrate hydrates and the first calculations of Xe shielding in a hydrogen-bonded system.

In this paper, we employ the dimer tensor model to represent the quantum mechanical Xe shielding tensor at arbitrary positions within a clathrate hydrate cage and use Monte Carlo simulations to calculate the NMR spectra of the Xe atoms occupying each of the 12 types of cages in four types of clathrate hydrate structures: structures I, II, H, and bromine hydrate.

METHODS

Quantum mechanical calculations of Xe shielding response

The models, the basis functions, the shielding calculations, the coordinates of the clathrate hydrate atoms, were introduced and described in Ref. 24. In the present work, we consider only the results from using the XCAGE/PCA model, in which the Xe atom in a cage in a crystal fragment is modeled by the Xe atom in the cage of water molecules, together with their full set of hydrogen-bonding partners, immersed in the point charge array that represents the remaining water molecules of the crystal. The point charge array self-consistently reproduces the Madelung potential in the region including the Xe atom and the cage (or extended cage) under investigation. For the present paper we use the results of the shielding tensor calculations using the DFT/B3LYP method.

The additive dimer tensor model

The model of additive dimer shielding tensors proposed by one of us in Ref. 17 assumes that it is possible to express each component of the symmetric shielding tensor of Xe in a particular configuration of neighboring A atoms in terms of a sum over contributions from Xe–A dimer tensor components: For example, for Xe in a channel of Ne atoms, the contribution to the Xe shielding due to the ith Ne atom located at (x_i,y_i,z_i) is given by the *ab initio* tensor component, the function $(\sigma_{\perp},\sigma_{\perp},\sigma_{\parallel})_{\mathrm{XeNe}}$ evaluated at r_{XeNe}. The derived expressions turn out to be simple geometric factors coupled with $\sigma_{\perp}$ and $\sigma_{\parallel}$ evaluated at r_{XeNe}. For example,

$$\sigma_{XX}=[(x_i-x_J)/r_{iJ}]^2\sigma_{\parallel}+\{[(y_i-y_J)/r_{iJ}]^2+[(z_i-z_J)/r_{iJ}]^2\}\sigma_{\perp}, \quad (1)$$

$$\tfrac{1}{2}(\sigma_{XY}+\sigma_{YX})=[(x_i-x_J)/r_{iJ}]\cdot[(y_i-y_J)/r_{iJ}](\sigma_{\parallel}-\sigma_{\perp}). \quad (2)$$

Terms like these are summed to include all the atoms in the channel. Then the shielding response in an external magnetic field (B_0) along a particular chosen direction (θ,ϕ) with respect to the crystal frame can be calculated as follows:

$$\begin{aligned}\sigma_{B0}(\theta,\phi)=&\sigma_{XX}\sin^2\theta\cos^2\phi+\sigma_{YY}\sin^2\theta\sin^2\phi\\&+\sigma_{ZZ}\cos^2\theta+\tfrac{1}{2}(\sigma_{XY}+\sigma_{YX})\sin^2\theta\sin 2\phi\\&+\tfrac{1}{2}(\sigma_{XZ}+\sigma_{ZX})\sin 2\theta\cos\phi\\&+\tfrac{1}{2}(\sigma_{YZ}+\sigma_{ZY})\sin 2\theta\sin\phi. \quad (3)\end{aligned}$$

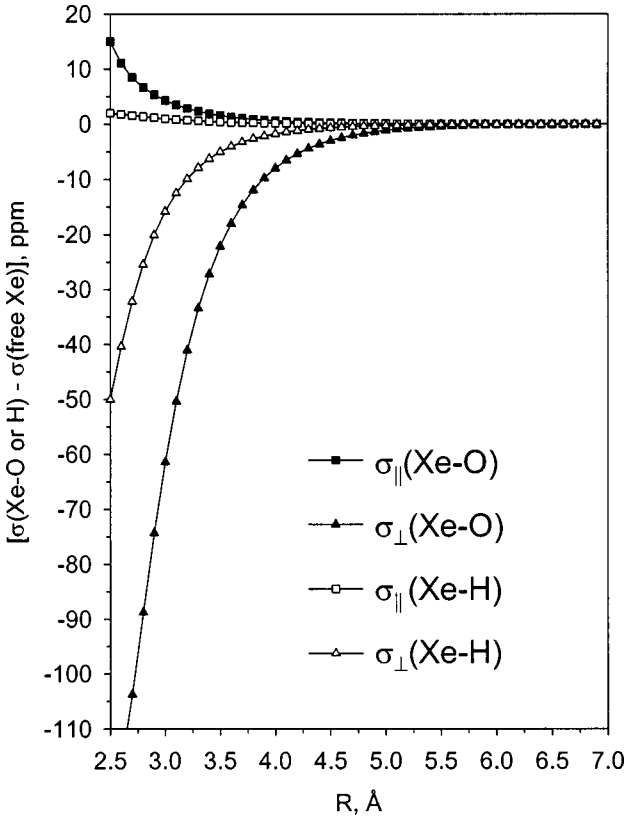

FIG. 1. The dimer shielding tensors $\sigma_{\parallel}$(Xe–O) and $\sigma_{\perp}$(Xe–O), $\sigma_{\parallel}$(Xe–H) and $\sigma_{\perp}$(Xe–H) obtained from fitting to the *ab initio* values of the Xe shielding tensor components.

The Xe tensor components $\sigma_{\parallel}$(Xe–O) and $\sigma_{\perp}$(Xe–O) and analogous ones for Xe–H atom pairs are shown in Fig. 1. These were obtained by fitting the calculated Xe shielding tensor components obtained from the DFT/B3LYP calculations using the XCAGE/PCA model to sums of Eq. (1) as follows:

$$\begin{aligned}\sigma_{XX}=&\Sigma_{O\,i}([X_{O\,i}-X_{Xe})/r_{i\,Xe}]^2\sigma_{\parallel}(r_{i\,Xe})\\&+\{[(Y_{O\,i}-Y_{Xe})/r_{i\,Xe}]^2+[(Z_{O\,i}-Z_{Xe})/r_{i\,Xe}]^2\}\\&\times\sigma_{\perp}(r_{i\,Xe}))+\Sigma_{H\,k}([(X_{H\,k}-X_{Xe})/r_{k\,Xe}]^2\sigma_{\parallel}(r_{k\,Xe})\\&+\{[(Y_{H\,k}-Y_{Xe})/r_{k\,Xe}]^2+[(Z_{H\,k}-Z_{Xe})/r_{k\,Xe}]^2\}\\&\times\sigma_{\perp}(r_{k\,Xe})),\end{aligned}\tag{4}$$

and independently to sums of Eq. (2) as follows:

$$\begin{aligned}\tfrac{1}{2}(\sigma_{XY}+\sigma_{YX})=&\Sigma_{O\,i}([(X_{O\,i}-X_{Xe})/r_{i\,Xe}]\\&\cdot[(Y_{O\,i}-Y_{Xe})/r_{i\,Xe}](\sigma_{\parallel}-\sigma_{\perp})(r_{i\,Xe}))\\&+\Sigma_{H\,k}([(X_{H\,k}-X_{Xe})/r_{k\,Xe}]\\&\cdot[(Y_{H\,k}-Y_{Xe})/r_{k\,Xe}](\sigma_{\parallel}-\sigma_{\perp})(r_{k\,Xe})),\end{aligned}\tag{5}$$

where $r_{i\,Xe}=r(\text{Xe–O}_i)$ and $r(\text{Xe–}H_k)$ and X, Y, and Z are the coordinates in the laboratory frame used to express the configuration of atoms in the crystal. Analogous equations are used for the other tensor components. One set of functions $\sigma_{\parallel}$(Xe–O), $\sigma_{\perp}$(Xe–O), $\sigma_{\parallel}$(Xe–H), and $\sigma_{\perp}$(Xe–H) is employed to fit all six tensor components of Xe calculated quantum mechanically for a large number of configurations of atoms. The resulting $\sigma_{\parallel}$(Xe–O), $\sigma_{\perp}$(Xe–O), $\sigma_{\parallel}$(Xe–H), and $\sigma_{\perp}$(Xe–H) functions are the functions shown in Fig. 1, each of which is in terms of inverse even powers of $r_{\text{Xe–O}}$ and $r_{\text{Xe–H}}$ from -6 to -12, with the coefficients determined by fitting to all *ab initio* components together. The quality of the fitting is shown in Fig. 2, where each *ab initio* tensor component value is plotted against the value reconstructed by using the dimer tensor model. The deviations seen in Fig. 2 include deviations from additivity assumed in the dimer tensor model as well as the inadequacy of the functional form used for the dimer shielding tensor functions. It should be noted that imperfect fitting leads to $[\sigma_{\parallel}(\text{Xe–O})+2\sigma_{\perp}(\text{Xe–O})]$ not exactly equal to $3\sigma_{iso}(\text{Xe–O})$, and $[\sigma_{\parallel}(\text{Xe–H})+2\sigma_{\perp}(\text{Xe–H})]$ not exactly equal to $3\sigma_{iso}(\text{Xe–H})$, where $\sigma_{iso}(\text{Xe–O})$ and $\sigma_{iso}(\text{Xe–H})$ are the isotropic shielding functions resulting from the fitting to the *ab initio* isotropic shielding values. The imperfect partitioning of the oxygen and hydrogen contributions to the shielding leaves the parallel and perpendicular components for each contribution somewhat less reliable than the individual isotropic shielding functions. Thus, the isotropic averages obtained by the line shape calculations using the functions $\sigma_{\parallel}$(Xe–O), $\sigma_{\perp}$(Xe–O), $\sigma_{\parallel}$(Xe–H), and $\sigma_{\perp}$(Xe–H) reported here slightly differ from the isotropic averages obtained by using the functions σ_{iso}(Xe–O) and σ_{iso}(Xe–H) reported in our previous paper, but only by tenths of a ppm or so.[24]

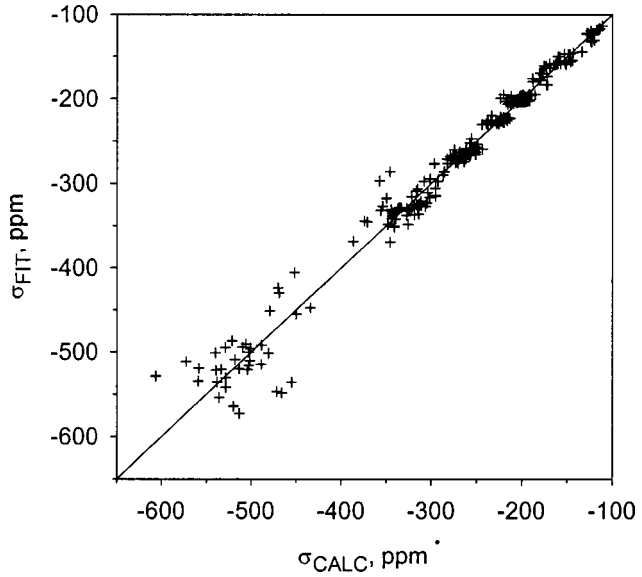

FIG. 2. The quality of the fit of all *ab initio* tensor components to the dimer tensor model.

Monte Carlo simulations

The supercells which are used as the simulation boxes for the simulations in this work are the same ones generated in Ref. 24. The method for obtaining the line shapes by Monte Carlo simulations of Xe in a supercell of a clathrate hydrate is that developed by one of us.[17] The approach is described in Ref. 17 for grand canonical ensembles. A poly-

crystalline sample in the B_0 magnetic field of an NMR spectrometer is represented by a single crystal fragment (the simulation box) stationary in the laboratory frame, while the constant B_0 field is permitted to change its orientation with respect to the laboratory frame. A set of 580 B_0 orientations (θ,ϕ) is chosen in such a way as to have uniform sampling of orientations. The polycrystalline powder line shape results when the ensemble averages of Eq. (3), $\langle \sigma^{B0}(\theta,\phi)\rangle$, are binned into a histogram. The finite number of orientations limits the practical resolution of the simulated line shape. Unlike the grand canonical simulations of Xe in ALPO-11, the Xe is not permitted to leave the cage where it is placed. All the $\sigma^{B0}(\theta,\phi)$ contributions for a given (θ,ϕ) from all the Xe atoms in the simulation box are accumulated together throughout the simulation. The frequency associated with the center of each bin of the coarse histogram resulting from the Monte Carlo simulations is assigned a Lorentzian line shape with a fixed line width to generate a ^{129}Xe spectrum. The bin width used in all the simulations reported here is 0.625 ppm, so the average shielding components can only be known to ± 0.3125 ppm. For display of the spectra, a Lorentzian linewidth of 0.5 ppm is used for the signals that correspond to less than five bins in the histogram and 1.5 ppm for all others. The average values for the individual six (in the most general case) components σ_{XX}, etc., are also part of the output, and permit us to examine the numerical values of the principal components and also the orientations of the principal axes of the tensor with respect to the crystal axes.

The potential functions used in the canonical Monte Carlo simulations for the present work are the same as those we used in Ref. 24. The Xe–Xe contributions to the calculated average shielding were neglected. Pairwise additive potentials of the Maitland–Smith form[25] were used,

$$V=\epsilon\left\{\frac{6}{n-6}\bar{r}^{-n}-\frac{n}{n-6}\bar{r}^{-6}\right\},$$

where n is allowed to vary with $\bar{r}=r/r_{\min}$ according to $n=m+\gamma(\bar{r}-1)$. For the Xe–O potential we used $m=13$, $\gamma=5$, $\epsilon/k=105.42$ K, $r_{\min}=3.724$ Å. For the Xe–H potential we used $m=13$, $\gamma=9.5$, $\epsilon/k=73.07$ K, $r_{\min}=3.471$ Å. We do not explicitly include induction terms in our potential; no charges are involved in the Monte Carlo averaging of the Xe shielding tensor. All atoms in the simulation box and their periodic images are treated as atoms in the Monte Carlo canonical averaging. Since the Xe–O and Xe–H parallel and perpendicular shielding functions correctly approach zero at large distances, cut-and-shifted shielding functions are used in parallel with cut-and-shifted potential functions.[26,27] The atoms beyond the first shell of water molecules hydrogen bonded to the water molecules of the cage containing the Xe atom lie at distances greater than the shielding cutoff distance so that the use of the XCAGE/PCA model for the shielding tensor calculations is completely consistent with the simulation techniques used.

Monte Carlo lineshape simulations were first carried out for a single Xe atom in a single XCAGE for each of the four types of cages: 5^{12} and $5^{12}6^2$ in structure I, and 5^{12} and $5^{12}6^4$ in structure II. The final averages reported here are calculated using a supercell under periodic boundary conditions as the simulation box. Supercells containing $4\times4\times4$ unit cells of clathrate hydrate structure I and $2\times2\times2$ unit cells of clathrate hydrate structure II were used. Only those cages in the supercell that have the same orientation with respect to the laboratory frame are filled with Xe atoms (three $5^{12}6^2$ cages in structure I and four 5^{12} cages in II), since we do not wish to simulate fast exchange of Xe atoms from cage to cage within the crystal, yet we wish to sample many proton distributions such as would result from proton dynamics with oxygen atoms remaining in place.

RESULTS

Xe shielding tensors at the centers of the cages in structures I and II

In Table I we compare the calculated Xe shielding tensor components [column (a)] at the center of each of the four cages in structures I and II with the tensor obtained from the dimer shielding tensor model [column (b)] at the center of each cage. Here we express our calculated values in terms of the Xe chemical shift rather than the shielding tensor components. The conversion is as follows:

$$\langle\delta_{\parallel}\rangle_{\mathrm{CALCD}}=[\sigma(\text{free Xe atom})-\langle\sigma_{\parallel}\rangle]/[1-\sigma(\text{free Xe atom})], \quad (6)$$

$$\langle\delta_{\perp}\rangle_{\mathrm{CALCD}}=[\sigma(\text{free Xe atom})-\langle\sigma_{\perp}\rangle]/[1-\sigma(\text{free Xe atom})]. \quad (7)$$

In Table I, comparison of column (a) with column (b) shows that deviations of the additive dimer tensors from the quantum-mechanical values to which they have been fitted do reflect the many-body terms not included in the model and also the inadequacies of fitting to a finite series in inverse powers of distance. Nevertheless, we see that the additive dimer tensor model provides a reasonable representation of the intrinsic anisotropy of the Xe environment reflected in the tensor calculated using DFT/B3LYP in XCAGE/PCA. The dimer tensor functions obtained from fitting the Xe tensors in structure I provide a good accounting of the tensors for Xe located at the centers of the cages of structures I and II in column (b) when compared to the actual *ab initio* values given in column (a).

The Xe tensors at the centers of all four types of cages are anisotropic, reflecting the specific proton configuration of the extended cage. However, in structure I, the $5^{12}6^2$ cage has a clearly greater anisotropy than the 5^{12} cage. Likewise, in structure II, the 5^{12} cage has a clearly greater anisotropy than the $5^{12}6^4$ cage. We note that the specific proton configuration of the XCAGE leads to a slightly anisotropic tensor at the center of the 5^{12} cage of type I with a span of 9.0 ppm; similarly the tensor at the center of the $5^{12}6^4$ cage of type II has a span of 4.9 ppm. Although the oxygen atoms of the $5^{12}6^2$ in structure I and 5^{12} in structure II form inherently axially symmetric cages, the specific proton configuration of a given XCAGE leads to a more general type of tensor with parallel component 91.6 ppm while the perpendicular components differ by 7.7 ppm for Xe in the $5^{12}6^2$ cage in structure I. We find similar tensor asymmetry in the 5^{12} cage in

TABLE I. ^{129}Xe chemical shift tensor principal components in clathrate hydrate structures I and II, given in ppm relative to free Xe atom, calculated by (a) single point *ab initio* calculation with Xe at the center of the cage using DFT/B3LYP, (b) calculated from the dimer shielding tensor model at the center of the cage, (c) Monte Carlo average using shielding tensor functions of Fig. 1 in a single XCAGE, (d) Monte Carlo average using dimer shielding tensor functions of Fig. 1 in all cages of a given type in a supercell of 4×4×4 unit cells for structure I and 2×2×2 unit cells for structure II. Lattice parameters at 275 K were used and Monte Carlo simulations were carried out at 275 K.

Chemical shift tensor component	At the center		Monte Carlo average	
	(a)	(b)	(c)	(d)
5^{12} cage of I	*Ab initio*	Dimer tensor model	Single XCAGE	128 cages
$\delta_{\parallel}$	194.4	195.8	214.8	214.05
$\delta_{\perp}$	200.4	196.9	214.1	213.96
$\delta_{\perp}$,	203.4	197.2	214.2	213.93
δ_{iso}	199.4	196.6	214.4	213.98
span	9.0	1.4	0.7	0.1
$5^{12}6^2$ cage of I	*Ab initio*	Dimer tensor model	Single XCAGE	384 cages
$\delta_{\parallel}$	91.6	103.6	134.0	133.19
$\delta_{\perp}$	116.9	118.4	155.1	153.83
$\delta_{\perp}$,	124.6	119.3	155.6	153.81
δ_{iso}	111.0	113.8	148.2	146.94
span	33.0	15.7	21.6	20.63
5^{12} cage of II	*Ab initio*	Dimer tensor model	Single XCAGE	128 cages
$\delta_{\parallel}$	173.4	175.8	195.9	194.33
$\delta_{\perp}$	194.1	195.2	215.6	213.84
$\delta_{\perp}$,	201.3	195.1	215.2	213.61
δ_{iso}	189.6	188.7	208.9	207.26
span	27.9	19.4	19.7	19.5
$5^{12}6^4$ cage of II	*Ab initio*	Dimer tensor model	Single XCAGE	64 cages
$\delta_{\parallel}$	43.2	53.9	103.5	104.59
$\delta_{\perp}$	45.6	54.2	104.5	104.70
$\delta_{\perp}$,	48.1	54.4	104.8	104.72
δ_{iso}	45.3	54.2	104.2	104.67
span	4.9	0.5	1.3	0.1

structure II; the perpendicular components differ by 7.2 ppm. These are a physical consequence of using a single cage with a specific static proton configuration.

Average Xe shielding tensors in structures I and II

Averaging over a large number of Xe positions within a given cage is necessary to correctly reflect the anisotropy of the shielding response at the Xe nucleus of a mobile Xe atom. Since the Xe atom has a finite probability of being found in a fairly large fraction of the free volume of the cage, the anisotropy that is observed experimentally in the lineshape could be different from the anisotropy of the Xe shielding tensor at the center of the cage, and may depend on the shape of the cavity. Shown in Fig. 3 are the Monte Carlo averaged spectra for Xe in the four cages in structures I and II obtained using the dimer shielding functions of Fig. 1 for Xe in a single extended cage (XCAGE) of each type of cage. The Xe chemical shift tensor components from these simulations are given in Table I column (c) and compared with the components obtained by Monte Carlo averaging in supercells containing cages with varying proton configurations in column (d). The results from averaging in $128\,5^{12}$ cages in structures I and II can be compared under the same statistical conditions by using 4×4×4 unit cells for structure I and 2×2×2 unit cells for structure II. Accompanying these are $64\,5^{12}6^4$ cages in structure II and $348\,5^{12}6^2$ cages in structure I. Column (c) in Table I shows that averaging within a single XCAGE removes most of the anisotropy arising from the specific proton configuration. The results for the 5^{12} cage in structure I in column (d) show that averaging in 128 cages with different proton configurations leads to a nearly isotro-

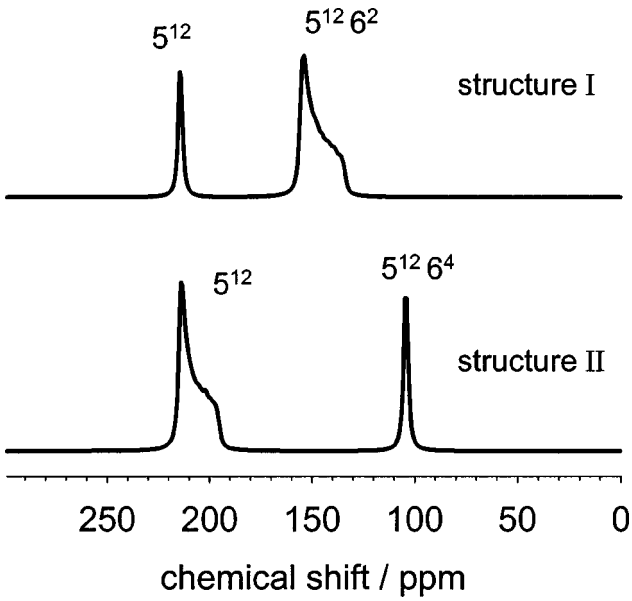

FIG. 3. The line shapes obtained by canonical Monte Carlo simulations of Xe in a single XCAGE of each of the four types of cages in clathrate hydrate structures I and II.

TABLE II. The average ^{129}Xe chemical shift tensor principal components in clathrate hydrates structures I and II, given in ppm relative to free Xe atom. Comparison of calculated values from MC simulations in supercells against experiment.

Chemical shift tensor component	T, K	5^{12} Structure I	$5^{12}6^2$ Structure I	5^{12} Structure II	$5^{12}6^4$ Structure II	Ref.
$\langle\delta_{\parallel}\rangle_{\mathrm{CALCD}}$	275	214.0	133.2	194.3	104.6	This work
$\langle\delta_{\perp}\rangle_{\mathrm{CALCD}}$	275	214.0	153.8	213.6	104.7	This work
$\langle\delta_{\perp'}\rangle_{\mathrm{CALCD}}$	275	214.0	153.8	213.8	104.7	This work
$\langle\delta_{\mathrm{iso}}\rangle_{\mathrm{CALCD}}$[a]	275	214.0	146.9	207.3	104.7	This work
$\mathrm{span}_{\mathrm{CALCD}}$	275	0.1	20.6	19.5	0.1	This work
$\delta_{\parallel\ \mathrm{EXPT}}$	200–240	242.0	130.7	213[b]	80[c]	5
$\delta_{\perp\ \mathrm{EXPT}}$		242.0	162.7	231[b]	80[c]	5
$\langle\delta_{\mathrm{iso}}\rangle_{\mathrm{EXPT}}$		242.0	152.0	225.0[b]	80[c]	5
$\mathrm{span}_{\mathrm{EXPT}}$		0	32	18[b]	0[c]	5
$\delta_{\parallel\ \mathrm{EXPT}}$	RT	244.6	135.7	217.6	THF[d]	11
$\delta_{\perp\ \mathrm{EXPT}}$		244.6	164.5	242.5	THF	11
$\langle\delta_{\mathrm{iso}}\rangle_{\mathrm{EXPT}}$		244.6	154.9	234.2	THF	11
$\mathrm{span}_{\mathrm{EXPT}}$		0	28.8	24.9	THF	11
$\delta_{\parallel\ \mathrm{EXPT}}$	RT			216.1	DCFE[e]	11
$\delta_{\perp\ \mathrm{EXPT}}$				239.65	DCFE	11
$\langle\delta_{\mathrm{iso}}\rangle_{\mathrm{EXPT}}$				231.8	DCFE	11
$\mathrm{span}_{\mathrm{EXPT}}$				23.55	DCFE	11

[a]These values are obtained from (1/3) the trace of the average tensor. On the other hand, using the shielding functions fitted to the isotropic *ab initio* values, we get, respectively, 214.1, 147.2, 207.0, and 104.9 ppm for these cages.
[b]Xe in a double hydrate type II in which *n*-propane occupies the $5^{12}6^4$ cage.
[c]The isotropic value is 86 ppm at 77 K, with benzene in the 5^{12} cage (Ref. 32).
[d]Xe in a double hydrate type II in which tetrahydrofuran occupies the $5^{12}6^4$ cage.
[e]Xe in a double hydrate type II in which 1,1,1-dichlorofluoroethane occupies the $5^{12}6^4$ cage.

pic average with a span of 0.1 ppm, much smaller than the 9.0 ppm calculated at the center of the same XCAGE. For the $5^{12}6^4$ cage of type II, columns (c) and (d) in Table I show that averaging within a single XCAGE removes most of the anisotropy. Averaging among 64 cages results in a tensor with a residual span of only 0.1 ppm, which is essentially isotropic.

Finally, we find nearly the same span for the average chemical shift tensors in the $5^{12}6^2$ cage of structure I and the 5^{12} cage of structure II. Averaging within a single $5^{12}6^2$ XCAGE leads to clearly axial tensors with the $\delta_{\parallel}$ smaller than $\delta_{\perp}$ in both cages. Averaging among 384 $5^{12}6^2$ cages in structure I gives results nearly identical to averaging within a single XCAGE. Similarly, averaging among 128 5^{12} cages of the supercell of structure II gives results nearly identical to those obtained by averaging within a single 5^{12} XCAGE. We carried out supercell calculations in order to ensure that the proton configurations are properly averaged over. As it turns out, for all four types of cages, averaging within a single XCAGE already provides nearly the same average tensor components as averaging in the supercell.

Comparison against experimental line shapes in structures I and II

The average Xe chemical shift tensor components obtained in this work from the supercell simulations are compared with experimental values in Table II. The theoretical spectra are displayed in Fig. 4, where they are compared with the Xe NMR spectra from the work of Ripmeester, Ratcliffe, and Tse.[5] In comparing our simulated line shapes with experiment, it should be noted that the ^{129}Xe NMR spectrum was observed in the Xe–propane hydrate structure II,[5] whereas we used the neutron diffraction data for the CCl_4 clathrate hydrate[28] to generate the coordinates of the supercell for our simulations. In addition, we have not taken into account any contributions to the Xe chemical shift from the molecules occupying the adjacent cages. There are well-known effects from occupancies of neighboring cages.[9,12] Nevertheless, the calculated line shapes are in reasonably good agreement with the experimental line shapes, as seen in Fig. 4. In summary, the spectra obtained from the simulations compare well with the corresponding experimental results at 77 K for Xe type I hydrate and the Xe–propane type II hydrate.[5]

The respective lineshapes for Xe@5^{12} and Xe@$5^{12}6^2$ in clathrate hydrate structure I are in accord with experiment. The ^{129}Xe spectrum for the symmetrical 5^{12} cage is isotropic as expected. Within our resolution (bin width of 0.625 ppm), the Xe@5^{12} has a signal indistinguishable from an isotropic line shape, with a span of 0.7 ppm in a single XCAGE with its specific proton configuration. A small span can arise from the small differences in the averages resulting from incompletely averaged proton configurations, even in the supercell. Our predicted span (21.6 ppm) for the $5^{12}6^2$ cage is somewhat smaller than the experimentally observed value (28.8–32 ppm). An axial anisotropy is consistent with the idealized symmetry of the $5^{12}6^2$ cage, which has a unique axis through the centers of the hexagonal faces. There is no apparent deviation from axial anisotropy in the line shape resulting from Monte Carlo simulations in the $5^{12}6^2$ cages of the supercell. Our simulations predict the unique component along the axis through the centers of the two hexagonal faces

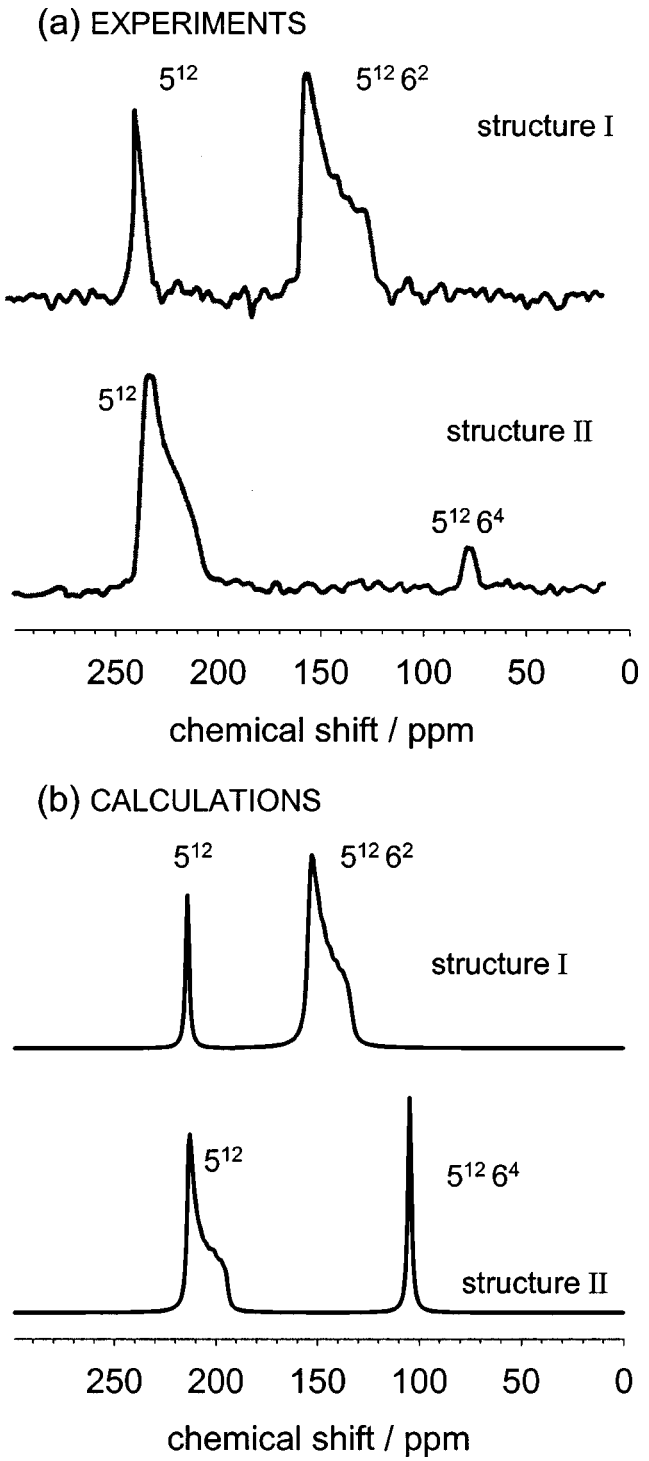

FIG. 4. The comparison of the calculated line shapes obtained from Monte Carlo simulations in supercells at 275 K with the experimental spectra of Xe in clathrate hydrate structures I and II from Ripmeester *et al.* for xenon type I hydrate and Xe–propane type II hydrate. The experimental spectra are reproduced from Ref. 5, with permission from the Royal Society of Chemistry. The numerical values for the tensor components are given in Table II.

to be less deshielded, whereas the two equivalent components perpendicular to this axis are more deshielded. This sign of the anisotropy had been predicted earlier without line shape calculations.[29]

The respective lineshapes for the Xe in the structure II supercell are also in accord with experiment. When the proton disorder is averaged out, the $5^{12}6^4$ cage is highly symmetrical (T_d), so it was not unexpected to find, for a single XCAGE, a span of 1.3 ppm which is just barely outside the resolution of our histogram (two adjacent bins). We therefore find an isotropic line shape even for simulations in a single XCAGE with its specific proton configuration. Averaging in an XCAGE results in very nearly the same tensor as averaging in the supercell. On the other hand, the 5^{12} cage in structure II is intrinsically less symmetrical than the 5^{12} cage in structure I when only the oxygen positions determined by neutron diffraction are considered, neglecting the proton disorder. The differences between the two types of 5^{12} cages are small and may be visualized by comparing O–O distances involving oxygen atoms opposite each other in the cages. Between the 5^{12} cages of structures I and II, the corresponding O–O distances differ by only 0.04 Å for six oxygen pairs; three differ by 0.11 and one by 0.05 Å. However, the 5^{12} cage in structure II has a unique axis, unlike the 5^{12} cage in structure I. If only the oxygen atoms are considered in the 5^{12} cage of structure II, there are two unique oxygen atoms through which an axis of symmetry can be drawn (see Fig. 5), whereas three pairs of such oxygen atoms can be chosen to form three such axes in the 5^{12} cage of structure I. Therefore, neglecting the protons, the 5^{12} cage of structure II should lead to an axially symmetric average tensor, whereas the 5^{12} cage of structure I should lead to an isotropic average tensor. The short Xe–O and Xe–H distances in both 5^{12} cages (I and II) lead to significant contributions from the highly deshielded portions of the Xe–O and Xe–H shielding functions, resulting in rather similar averages for the centroid of the peaks, but in the Monte Carlo averaging the Xe clearly distinguishes that the 5^{12} cage of structure II is less symmetrical than the 5^{12} cage in structure I. The short Xe-cage atom distances in the 5^{12} cages that correspond to the highly deshielded parts of the shielding functions merely amplify the differences between averages obtained at various directions of the B_0 field with respect to the crystal frame.

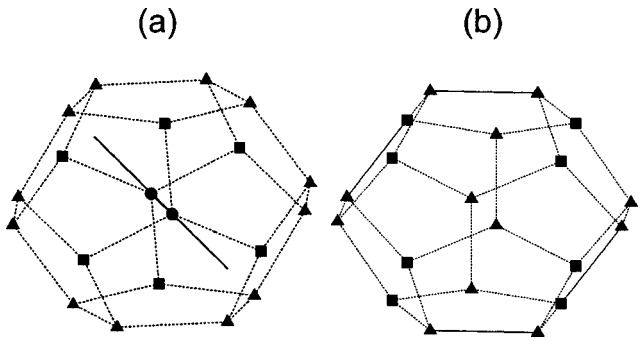

FIG. 5. In the idealized 5^{12} cage in clathrate hydrate structure II (a), a unique axis connects two unique oxygens, leading to an axially symmetric cage, in contrast to the 5^{12} cage in structure I (b).

Xe tensors in the cages of structure H

Clathrate hydrate type H consists of three types of cages: 5^{12}, $4^3 5^6 6^3$, and $5^{12}6^8$, and has been reported to be isostructural with hexagonal clathrasil D1H. Using the unit cell parameters of structure H from powder diffraction pattern[30]

and the structure of hexagonal clathrasil D1H from synchrotron diffraction,[31] we have obtained the coordinates of the oxygen atoms. The proton positions were assigned at 1.00 Å from the oxygen atoms along the edges of the polygons that make up the cages. We follow the same methods as we have developed for structures I and II, generating a simulation box containing a certain number of unit cells that obey the ice rules under periodic boundary conditions. Since we have discovered that supercell simulations provide nearly identical results as XCAGE simulations, we report only results of Monte Carlo simulations in an extended cage of each type using the same shielding functions and the same potential functions as for structures I and II. The results are shown in Fig. 6 where they are compared with the experimental results of Ripmeester *et al.*[5] The calculated lineshapes clearly show three distinct components for the Xe chemical shift tensor in the 5^{12} cage and axial tensors with opposite-signed anisotropies for Xe in the $4^3 5^6 6^3$ and $5^{12}6^8$ cages. The most general type of average Xe chemical shift tensor found for Xe atom in a 5^{12} cage is seen in structure H. The tensor has three distinct components and the isotropic value is shifted from the Xe tensor in the $4^3 5^6 6^3$ cage by about 7 ppm, as compared to the experimentally observed 17 ppm. The calculated Xe spectra in the 5^{12} and $4^3 5^6 6^3$ cages are completely consistent with the deconvolution proposed by Ripmeester *et al.*[5] for the combined peaks in the observed static powder spectrum. The NMR signal for Xe in the $5^{12}6^8$ cage has not been observed experimentally. The average Xe chemical shift tensor components for a Xe atom in the cages of structure H are given in Table III. We find excellent agreement with the experimental values with respect to the absolute chemical shifts measured from the free Xe atom and the anisotropies of each observed signal. The $5^{12}6^8$ cage which is elongated along the unique axis yields average Xe tensor components in the relative order $\langle \delta_{\parallel} \rangle > \langle \delta_{\perp} \rangle$. On the other hand, the disk-shaped $4^3 5^6 6^3$ cage yields Xe chemical shift tensor components in the relative order $\langle \delta_{\perp} \rangle > \langle \delta_{\parallel} \rangle$, just as the disk-shaped $5^{12}6^2$ cage of structure I. These relative orders of the parallel and perpendicular components for Xe chemical shift tensors of a Xe atom in oblate and prolate cages had been predicted by one of us, without line shape calculations, by considering the limiting cases of the shielding of a Xe atom in right circular and elliptical cylinders.[29]

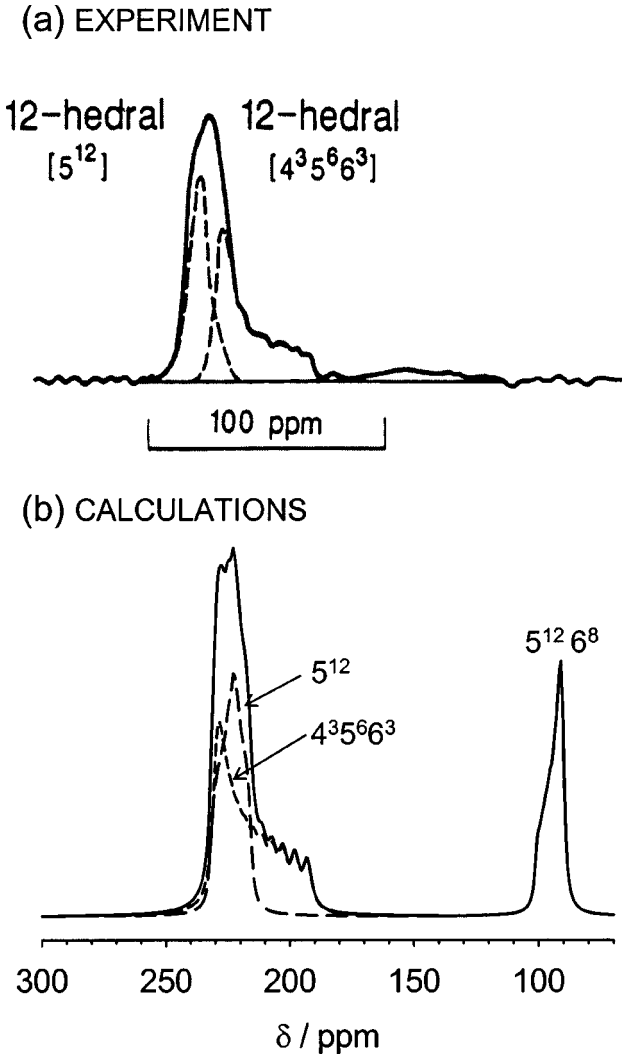

FIG. 6. The line shapes obtained by canonical Monte Carlo simulations of Xe in a single XCAGE of each of the three types of cages in clathrate hydrate structure H at 275 K are compared with the experimental line shapes from Ripmeester *et al.* for Xe–methylcyclohexane type H hydrate. The experimental spectra are reproduced from Ref. 5, with permission from the Royal Society of Chemistry. The numerical values for the tensor components are given in Table III.

Xe tensors in the cages of bromine hydrate

Bromine hydrate is a clathrate hydrate that has been known since 1829, but its structure was not definitely known until the work of Udachin *et al.* in 1997.[32] Their single crystal x-ray diffraction analysis reveals a water framework with unit cells consisting of $10\,5^{12}$ (D) cages, $16\,5^{12}6^2$ (T) cages, and four $5^{12}6^3$ (P) cages in the unit cell. Furthermore, there are two distinct types of D cages, $2D_A$ and $8D_B$ and two distinct types of T cages, $8T_A$ and $8T_B$ in the unit cell. ^{129}Xe NMR spectroscopy in double hydrates of xenon and Br_2 provide results that are consistent with the tetragonal structure from single crystal x-ray diffraction.[32]

We follow the same methods as for structures I and II, generating a simulation box of $2\times2\times2$ unit cells that obey the ice rules under periodic boundary conditions. With the unit cell parameters and the fractional coordinates of water oxygens given in Ref. 32, we have obtained the coordinates of the oxygen atoms. As for clathrate H, the proton positions were assigned at 1.00 Å from the oxygen atoms along the edges of the polygons that make up the cages. We report results of Monte Carlo simulations in an extended cage of each type using the same shielding functions and the same potential functions as we have used for structures I and II. The calculated tensor components are shown in Table IV which provides a comparison of the static and magic angle spinning (MAS) ^{129}Xe results from Udachin *et al.*[32] with our Monte Carlo simulations. In Fig. 7 our calculated line shapes are compared with the experimental spectra.[32]

In our canonical Monte Carlo simulations we do not determine the relative distribution of Xe among the types of cages, so the calculated relative intensities of the lines observed for Xe in the 5^{12}, $5^{12}6^2$, and $5^{12}6^3$ cages only represent the number of cages of each type in the crystal of bro-

TABLE III. The ^{129}Xe chemical shift tensor in clathrate hydrate structure H, given in ppm relative to free Xe atom. Calculations (this work) were done at 275 K; experiments (Refs. 1 and 6) were done at 220–240 K.

	5^{12}	$4^3 5^6 6^3$	$5^{12}6^8$
$\langle\delta_{\parallel}\rangle_{\mathrm{CALCD}}$	217.5	190.7	99.6
$\langle\delta_{\perp}\rangle_{\mathrm{CALCD}}$	224.1	230.3	89.8
$\langle\delta_{\perp'}\rangle_{\mathrm{CALCD}}$	233.3	230.6	89.1
$\langle\delta_{\mathrm{iso}}\rangle_{\mathrm{CALCD}}$[a]	224.9	217.2	92.8
$\mathrm{span}_{\mathrm{CALCD}}$	15.8	40	10.5
$\delta_{\mathrm{iso\ EXPT}}$[b]	232	215	
$\mathrm{span}_{\mathrm{EXPT}}$[b]	<5	~ 40	

[a]These values are obtained from (1/3) the trace of the average tensor. On the other hand, using the shielding functions that have been fitted to the isotropic *ab initio* values, we obtain isotropic chemical shifts of 223.5, 214.7, and 91.4 ppm, respectively, for these cages.
[b]References 5 and 10.

mine hydrate. The Monte Carlo simulations provide line shapes which are completely consistent with experiment. The simulations can distinguish between the inequivalent D_A and D_B cages (5^{12}) and the inequivalent T_A and T_B cages ($5^{12}6^2$). The Xe chemical shift tensor in the D_A cages have a larger anisotropy than the tensor in the D_B cages, but since the ratio 2:8 is rather unfavorable for the D_A cages, the overlapping line shapes observed has an apparent anisotropy closer to that of the Xe tensor in the D_B cages. The equal numbers of T_A and T_B cages would lead to overlapping spectra that have an apparent span closer to that of the T_A cage, if the *A* and *B* cages are equally likely to be occupied. Overall, the complete Xe NMR spectrum for bromine hydrate with xenon is in excellent agreement with the experiments.

The Xe signal from the *P* cage was not observed by Udachin *et al.*, however, they expected it to appear somewhere between the $5^{12}6^2$ of structure I and the $5^{12}6^4$ of structure II, and to be anisotropic.[32] Indeed, we find that their qualitative predictions agree completely with our calculated results for Xe in the $5^{12}6^3$ cage. We found only a small anisotropy in averaging using the $5^{12}6^3$ XCAGE model in the simulations.

General considerations of the average Xe shielding tensor in a cage as a signature of the cage structure

The nuclear site symmetry at the center of the cage, ignoring the proton positions, can provide the number of unique shielding tensor components for Xe at that position, and these are known from group theoretical considerations in the work of Buckingham and Malm.[33] At arbitrary locations other than the center of the idealized cage, the Xe tensor is generally asymmetric, however, with as many as six distinct components. How then do the average shielding tensors for the Xe atom in a cage come to reflect the idealized cage symmetry? In the Monte Carlo averaging, the one-body distribution function of the Xe atom in a cage, ignoring the proton positions, should reflect the crystallographic symmetry of the cage. For this reason, equivalent positions in space with asymmetric instantaneous tensors end up with cancellation of opposite signed off-diagonal elements, since the probability of finding the Xe in equivalent locations are equal, leaving only the noncanceling parts to survive. The use of the dimer tensor model permits the analysis to be transparent in Eqs. (4) and (5). In this additive approximation, the off-diagonal components of the tensor change sign for equivalent positions which are related by symmetry operations such as rotation about a symmetry axis, reflection through a mirror plane, or inversion through the origin (the center of the cage). Thus, when the average is taken over a large number of Metropolis-weighted Xe positions within the cage, the uniform sampling over equivalent positions leads to cancellation of contributions. Because the averaging leads to cancellation of equal and oppositely signed terms, despite the fact that the symmetric part of the *ab initio* Xe shielding tensor at each arbitrary position within the cage (other than the center) is a general six-component tensor, the resulting

TABLE IV. The ^{129}Xe chemical shift tensors in clathrate xenon bromine double hydrate, given in ppm relative to free Xe atom. Calculations were done at 275 K (this work); experiments were done at 77 and 245 K (Ref. 32).

	5^{12} (D_A)	5^{12} (D_B)	$5^{12}6^2$ (T_A)	$5^{12}6^2$ (T_B)	$5^{12}6^3$ (P)
$\langle\delta_{\parallel}\rangle_{\mathrm{CALCD}}$	216.4	218.2	132.5	134.2	129.4
$\langle\delta_{\perp}\rangle_{\mathrm{CALCD}}$	237.3	232.3	149.0	146.3	125.2
$\langle\delta_{\perp'}\rangle_{\mathrm{CALCD}}$	245.8	233.4	155.7	148.6	126.6
$\langle\delta_{\mathrm{iso}}\rangle_{\mathrm{CALCD}}$[a]	233.2	228.0	145.8	143.0	127.1
$\mathrm{span}_{\mathrm{CALCD}}$	29.3	15.1	23.2	14	4.2
$\delta_{\mathrm{iso\ EXPT}}$[b] at 245 K MAS	256	253	153	153	c
$\delta_{\mathrm{iso\ EXPT}}$[b] at 77 K static	244		~ 147		c
$\mathrm{span}_{\mathrm{EXPT}}$[b] at 77 K	~ 25[d]		~ 35[d]		

[a]These values are obtained from (1/3) the trace of the average tensor. On the other hand, using the shielding functions fitted to the isotropic *ab initio* values, we obtain 232.4, 227.7, 145.9, 143.7, and 127.7 ppm, respectively, for these cages.
[b]Reference 32.
[c]Either Xe is not competitive with Br_2 for this cage or else the peak is overlapping with the peak at 153 ppm assigned to the *T* cages (Ref. 32).
[d]Estimated from the spectra in Fig. 8 of Ref. 32.

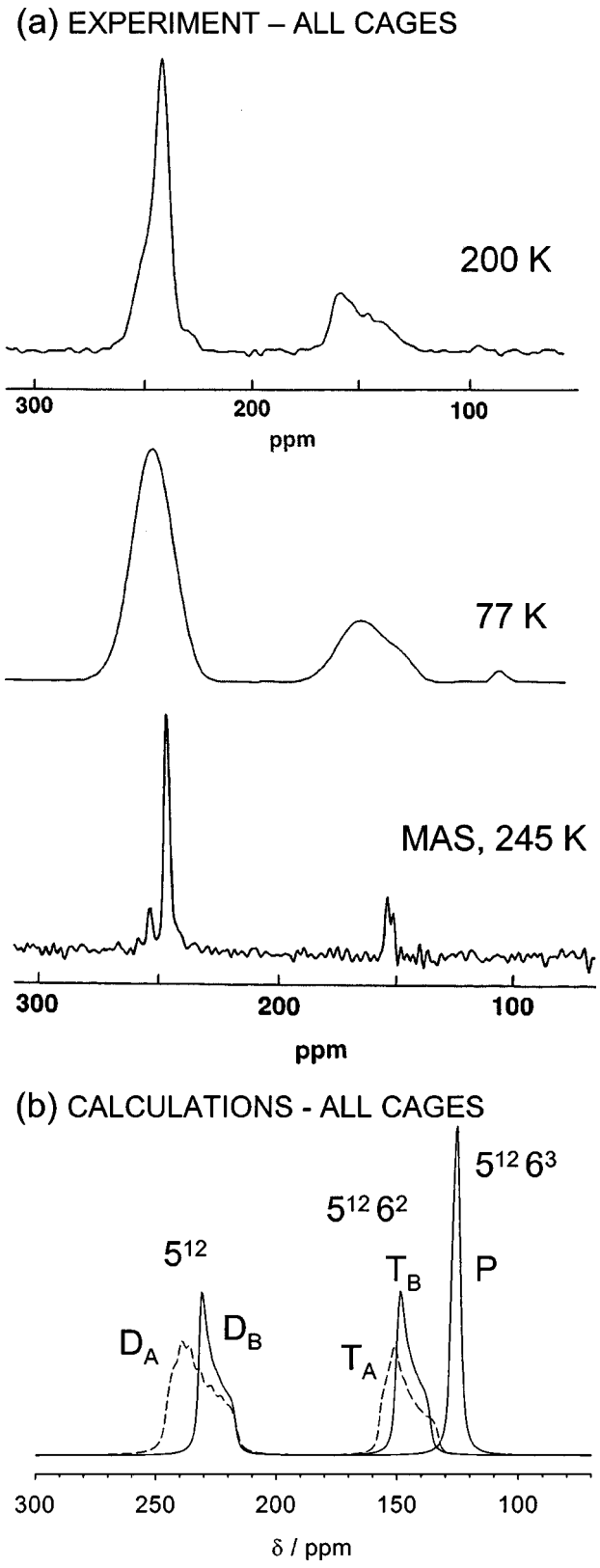

FIG. 7. The line shapes obtained by canonical Monte Carlo simulations of Xe in a single XCAGE of each of the five types of cages in bromine hydrate at 275 K are compared with the experimental line shapes at 77 K and 200 K from Udachin *et al.* (Ref. 32). The MAS experiment suggests two types of cages D_A, D_B and T_A, T_B. The experimental spectra are reproduced from Ref. 32, with permission from the American Chemical Society. The numerical values for the tensor components are given in Table IV.

Monte Carlo average Xe shielding tensors will reflect the symmetry of the cage itself. This is a particularly strikingly demonstrated in the cases where there are only one or two unique tensor components in the average tensor. *Thus, we arrive at an extremely useful conclusion, that the number of unique tensor components can be predicted a priori for a single Xe atom in a cage directly from the symmetry of the cage itself.* In the clathrate hydrate, the disorder of proton positions imposes an additional complication in that frozen positions lower the symmetry of the cages. However, the asymmetry arising from only including a finite number of specific proton positions does not give significant contributions. Ripmeester and co-workers were the first to recognize that the observed Xe line shapes exhibit axial anisotropy for those cages which have a unique symmetry axis.[5,7]

Table V summarizes the tensor symmetry predictions from Buckingham and Malm[29] for the nuclear site symmetry at the center of the 12 cages in structures I, II, H, and bromine hydrate. The average tensors from our Monte Carlo simulations in these cages have the expected number of unique components, and the principal axis directions found for the average tensor are the expected ones, corresponding to the symmetries of the idealized cages, within the statistical errors of the simulations. We do indeed find that our results bear out the general consequence of symmetry arising from averaging the shielding over the one-body distribution of Xe in the cage.

In Figs. 8–10 we provide a summary of the assignments of our calculated average tensor components to the cage axes in the various clathrate hydrates. Since we use the coordinates of the cage atoms in our Monte Carlo simulations, the average tensor components that result from the simulations can be associated unequivocally with the crystal axes and the axes of the individual cages. In Fig. 8, the $5^{12}6^2$ cage in structure I is clearly axially symmetric. There are three types of these cages with the unique axis lined up along each of the crystallographic axis. One of the principal axes (the unique one at 194 ppm) of the Xe tensor in the 5^{12} cages of structure II is shown in better detail in Fig. 5. The other two principal components are orthogonal to this and equivalent to each other (214 ppm). Where there is a unique axis for the cage, as in the $5^{12}6^2$ cage of structure I (Fig. 8) and the $4^3 5^6 6^3$ cage in structure H (Fig. 9), the observation of an axial tensor is expected. In such cases, the assignments are obvious from the experimental spectra. The $5^{12}6^8$ cage in structure H is apparently not populated by Xe, but we predict an axially symmetric tensor with the higher chemical shift along the unique axis which is the sixfold symmetry axis (the long axis of the cage). The 5^{12} cage of structure H has three unique components, along the three twofold axes of the cage (D_{2h}), but they are not greatly different from each other. Only the principal values are shown when symmetry dictates more than three unique components of the tensor, although the calculations provide the full tensor for Xe in the Cartesian frame of the crystal in every case, including the off-diagonal elements.

The cages carved out of the bromine hydrate crystal[32] shown in Fig. 10 show unequivocally the *A* and *B* types of 5^{12} and $5^{12}6^2$ cages are different from each other. Despite

TABLE V. The symmetry-predicted number of unique Xe shielding tensor components for Xe in various types of idealized cages. The *X, Y, Z* indices are not associated with the crystal frame; the *Z* index corresponds to the highest-fold axis of symmetry of the cage, or else the unique twofold axis.

Cage type	Nuclear site symmetry at center of cage[a]	Unique tensor components at center, determined by symmetry[b]	Unique average components found by Monte Carlo simulations[c]
5^{12} in I	T_h	1: $\sigma_{ZZ}=\sigma_{XX}=\sigma_{YY}$	1: $\sigma_{ZZ}=\sigma_{XX}=\sigma_{YY}$
$5^{12}6^2$ in I	D_{2d}	2: σ_{ZZ}, $\sigma_{XX}=\sigma_{YY}$	2: σ_{ZZ},[d] $\sigma_{XX}=\sigma_{YY}$
5^{12} in II	D_{3d}	2: σ_{ZZ}, $\sigma_{XX}=\sigma_{YY}$	2: σ_{ZZ},[e] $\sigma_{XX}=\sigma_{YY}$
$5^{12}6^4$ in II	T_d	1: $\sigma_{ZZ}=\sigma_{XX}=\sigma_{YY}$	1: $\sigma_{ZZ}=\sigma_{XX}=\sigma_{YY}$
5^{12} in H	D_{2h}	3: σ_{ZZ}, σ_{XX}, σ_{YY}	3: σ_{ZZ}, σ_{XX}, σ_{YY}
$4^3 5^6 6^3$ in H	D_{3h}	2: σ_{ZZ}, $\sigma_{XX}=\sigma_{YY}$	2: σ_{ZZ},[f] $\sigma_{XX}=\sigma_{YY}$
$5^{12}6^8$ in H	D_{6h}	2: σ_{ZZ}, $\sigma_{XX}=\sigma_{YY}$	2: σ_{ZZ},[g] $\sigma_{XX}=\sigma_{YY}$
5^{12} (D_A) in bromine hydrate	D_{2h}	3: σ_{ZZ}, σ_{XX}, σ_{YY}	3: σ_{ZZ}, σ_{XX}, σ_{YY}
5^{12} (D_B) in bromine hydrate	D_{2h}	3: σ_{ZZ}, σ_{XX}, σ_{YY}	3: σ_{ZZ}, σ_{XX}, σ_{YY}
$5^{12}6^2$ (T_A) in bromine hydrate	C_s	4: σ_{ZZ}, σ_{XX}, σ_{YY}, σ_{XZ}	3[h]: σ_{ZZ}, σ_{XX}, σ_{YY}
$5^{12}6^2$ (T_B) in bromine hydrate	C_s	4: σ_{ZZ}, σ_{XX}, σ_{YY}, σ_{XZ}	3[h]: σ_{ZZ}, σ_{XX}, σ_{YY}
$5^{12}6^3$ (P) in bromine hydrate	C_{2v}	3: σ_{ZZ}, σ_{XX}, σ_{YY}	3: σ_{ZZ}, σ_{XX}, σ_{YY}

[a]From Ref. 1 for structures I, II, H, from Ref. 32 for the bromine hydrate.
[b]From Buckingham and Malm (Ref. 33). Only the components of the symmetric part of the shielding tensor are included in this column since the antisymmetric part of the shielding tensor is not directly observable in NMR experiments.
[c]Neglecting small differences that may be attributed to proton disorder. The assignments of the calculated average tensor components to the axis directions in the respective cages are given in Fig. 8.
[d]The unique component is along the line connecting the centers of the six-membered rings.
[e]The unique component is along the line connecting the pair of unique oxygens as shown in Fig. 5.
[f]The unique component is along the line connecting the vertices shared by three five-membered rings.
[g]The unique component is along the long axis of the cage.
[h]Only the principal tensor elements in the principal axis system manifest themselves in the NMR spectrum of polycrystalline samples such as the clathrate hydrates. The full tensor results from the simulations but this can be obtained only in a single crystal experiment.

the appearance of the cluster of $5^{12}6^2$ (T_A) cages displayed in Fig. 10 as stacked along the *z* axis of the crystal, the T_A cages have D_{2h} symmetry and cannot lead to an axially symmetric Xe tensor. There are three distinct components, in agreement with the symmetry rules of Buckingham and Malm.[33] On the other hand, the nearly axial symmetry of the Xe tensor in the $5^{12}6^2$ (T_B) cage is easily understood in the view shown at the bottom right of Fig. 10 (the cluster of T_B cages viewed from below). The larger two of the principal components, although statistically distinct, are nearly equal.

The theoretical calculations can provide assignment information not available from experiments on polycrystalline material, especially where overlapping peaks may occur and/or some cage types are not sufficiently populated by Xe to result in the observation of a characteristic line shape under normal conditions. In such cases theoretical calculations can provide a region where the weak signal may be expected to appear, for example, the $5^{12}6^8$ cage in structure H or the $5^{12}6^3$ cage in bromine hydrate, as well as a signature line shape to compare with and confirm the assignment.

Temperature dependence

We performed simulations at 77 and 275 K for Xe in clathrate hydrate structures I and II. The lattice parameters are known as a function of temperature from the work of Ikeda *et al.*[34] We used the appropriate lattice parameter to scale the coordinates between 77 and 275 K. The Xe one-body distribution is also a function of temperature and is determined by Monte Carlo simulations at the two temperatures. The results are compared in Table VI. The temperature dependence of the ^{129}Xe chemical shift tensors predicted in this work can be summarized as follows: The chemical shift span and the isotropic chemical shift both increase with increasing temperature for the larger cages ($5^{12}6^2$ cage in type I and $5^{12}6^4$ cage in type II), whereas they both decrease with increasing temperature for the smaller cages (5^{12} cages in type I and II). The changes with temperature are systematic, but not large. These changes are opposite to the temperature dependence expected in the limiting cases of small spherical cages and large spherical cages.

Let us consider the limiting cases of a small cage and a large cage. The different temperature behaviors of the chemical shift of a single Xe atom in a cage have to do with the potential energy surfaces, which in turn determine the one-body distribution function. In a small cage, the potential sur face has a minimum at the center of the cage. In a large cage, the center is a local maximum, and the lowest energy positions lie along a three-dimensional potential trough that is shaped by the walls of the cage. In a small cage, the highest probability of finding the Xe is at the center, at any temperature. At low temperatures, the one-body distribution is tightly peaked at the center. At higher temperatures, the one-body distribution function is still peaked at the center but the probability of finding Xe off center is increased, leading to increased contributions from highly deshielding close encounters with wall atoms. Therefore, the Xe chemical shift increases with increasing temperature in the limiting case of a small cage. In a large cage, at low temperatures, the highest

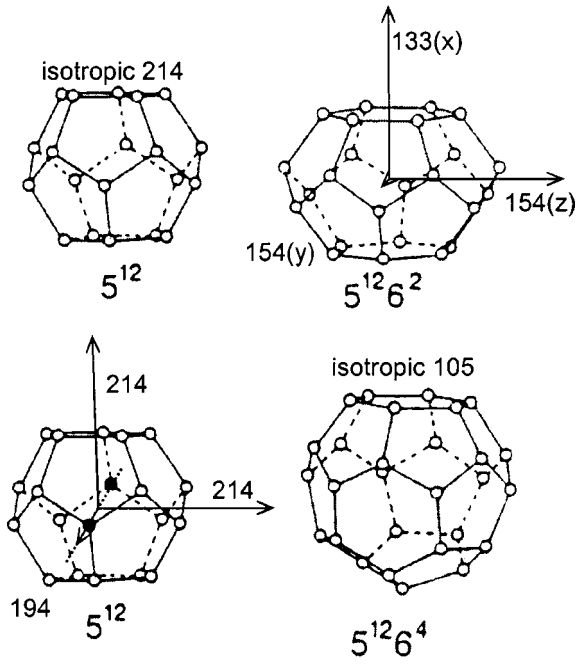

FIG. 8. The assignments of the calculated average tensor components (in Table II) to the axes for Xe in clathrate hydrate structures I and II. One of the principal axes for the Xe tensor in the 5^{12} cages of structure II is shown in Fig. 5, the unique one, corresponding to 194 ppm. The other two are orthogonal to this and equivalent to each other (214 ppm). Indicated in parentheses are the instances where the principal axes of the Xe chemical shift tensor are parallel to the *x*, *y*, or *z* crystal axes.

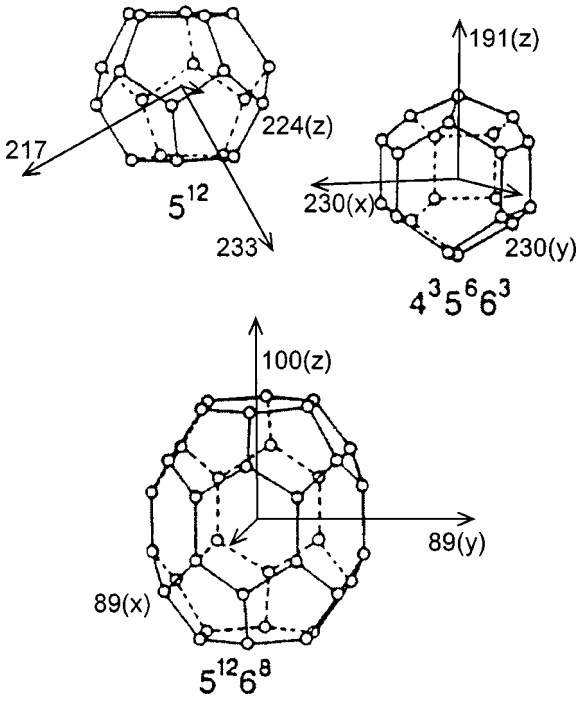

FIG. 9. The assignments of the calculated average tensor components (in Table III) and the orientation of the principal axes of the Xe chemical shift in clathrate hydrate H. Indicated in parentheses are the instances where the principal axes of the Xe chemical shift tensor are parallel to the *x*, *y* or *z* crystal axes.

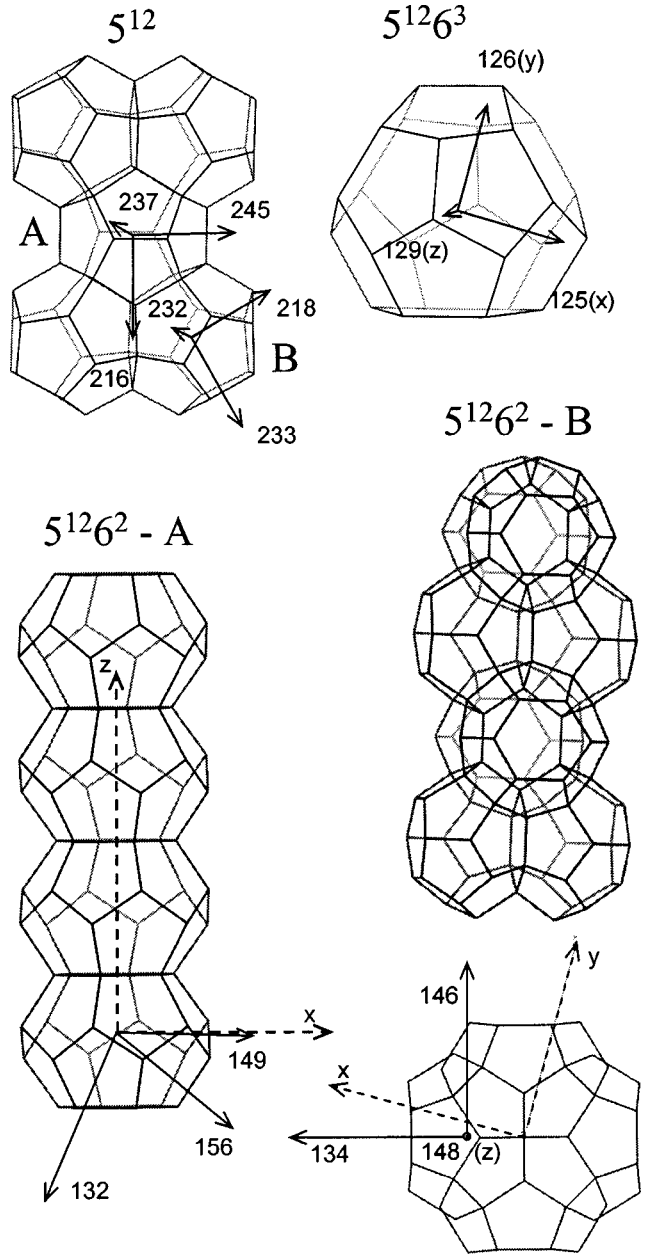

FIG. 10. The assignments of the calculated average tensor components and the orientation of the principal axes of the Xe chemical shift in bromine hydrate. To illustrate the orientation of the principal axes in the crystalline frame, we have reproduced the drawings of the cages from Ref. 32, with permission from the American Chemical Society. Indicated in parentheses are the instances where the principal axes of the Xe chemical shift tensor are parallel to the *x*, *y*, or *z* crystal axes.

probability of finding the Xe is along the trough, whereas the probability is smaller for finding Xe close to the center, where the deshielding contributions from the remote cage atoms are much smaller. At higher temperatures, the one-body distribution function is still highest along the trough but the probability of finding Xe close to the center is increased, leading to increased contributions from low deshielding terms of remote wall atoms. Therefore, the Xe chemical shift decreases with increasing temperature in the limiting case of a large cage. At some intermediate cage size, between these limiting cases, the Xe chemical shift tensor can be nearly temperature independent.

TABLE VI. The temperature dependence of the ^{129}Xe chemical shift tensor in the cages of clathrate hydrate structures I and II, using a single XCAGE for the simulation box for both temperatures.

	5^{12} Structure I	5^{12} Structure II	$5^{12}6^2$ Structure I	$5^{12}6^4$ Structure II	T, K
$\langle\delta_{\|}\rangle_{\mathrm{CALCD}}$	220.1	196.9	129.1	102.0	77
$\langle\delta_{\perp}\rangle_{\mathrm{CALCD}}$	219.4	217.7	149.0	102.9	77
$\langle\delta_{\perp'}\rangle_{\mathrm{CALCD}}$	219.4	217.9	149.8	103.2	77
$\langle\delta_{\mathrm{iso}}\rangle_{\mathrm{CALCD}}$[a]	219.6	210.8	142.6	102.7	77
$\mathrm{span}_{\mathrm{CALCD}}$	0.7	21.0	20.6	1.2	77
$\langle\delta_{\|}\rangle_{\mathrm{CALCD}}$	214.8	195.9	134.0	103.5	275
$\langle\delta_{\perp}\rangle_{\mathrm{CALCD}}$	214.1	215.6	155.1	104.5	275
$\langle\delta_{\perp'}\rangle_{\mathrm{CALCD}}$	214.2	215.2	155.6	104.8	275
$\langle\delta_{\mathrm{iso}}\rangle_{\mathrm{CALCD}}$[b]	214.4	208.9	148.2	104.2	275
$\mathrm{span}_{\mathrm{CALCD}}$	0.7	19.7	21.6	1.3	275
sign of $d\langle\delta\rangle/dT$	−	−	+	+	

[a]These values are obtained from (1/3) the trace of the average tensor. On the other hand, using the shielding functions fitted to the isotropic *ab initio* values, we obtain 220.0, 210.5, 143.0, and 103.1 ppm, respectively, for these cages at 77 K.

[b]These values are obtained from (1/3) the trace of the average tensor. On the other hand, using the shielding functions fitted to the isotropic *ab initio* values, we obtain 214.1, 207.9, 148.3, and 104.5 ppm, respectively, for these cages at 275 K.

These qualitative predictions of temperature dependence in the limiting small and large cage cases assume that the cage itself is static with temperature. In clathrate hydrate structures I and II, however, the lattice parameters increase systematically with increasing temperature, that is, the individual cages increase in size. All other factors (e.g., electronic structure of cage atoms) remaining the same, when the cage dimensions increase with increasing temperature, the average Xe chemical shift will decrease because, for corresponding Xe positions relative to the center, all Xe-cage atom distances become longer, leading to smaller deshielding. This is the trend found in our Monte Carlo simulations for both 5^{12} cage types in structures I and II (see Table VI), where a small increase in the cage dimensions can have a significant and dominant effect on the average Xe chemical shift, since the preponderant Xe–O and Xe–H distances are rather short. On the other hand, the $5^{12}6^2$ and $5^{12}6^4$ cages, though larger than the 5^{12} cages, are still fairly small cages, and exhibit the temperature dependence of the limiting case of the small pore (increasing Xe chemical shift with increasing temperature), despite the concomitant increase in cage dimensions with increasing temperature.

Although Xe chemical shifts in clathrate hydrate cages have been reported at various temperatures,[5–11] the variation of the ^{129}Xe isotropic chemical shifts and line shapes have not been systematically studied as a function of temperature. We compare our results with the separate reports of the isotropic Xe chemical shifts in the 5^{12} and $5^{12}6^2$ cages of structure I at both 275 K and at 77 K: For the 5^{12} cage Ripmeester and co-workers reported 242 ppm at 275 K,[7] and 250 ppm at 77 K.[32] The observed increase in Xe chemical shift with decreasing temperature in the 5^{12} cage of structure I is in the same direction as our simulations predict for this cage. In the same respective samples, the isotropic Xe chemical shifts in the $5^{12}6^2$ cages of structure I are reported as 152 ppm at 275 K,[7] and 148 ppm at 77 K.[32] The observed decrease in Xe chemical shift with decreasing temperature in the $5^{12}6^2$ cage of structure I is in the same direction as our simulations predict for this cage. On the other hand, the isotropic Xe chemical shift in the $5^{12}6^4$ cage of structure II has been reported as 80 ppm at 200–240 K,[5] and 86 ppm at 77 K.[32] The observed increase in Xe chemical shift with decreasing temperature in the $5^{12}6^4$ cage of structure II is in the opposite direction to that predicted by our simulations for this cage. However, it has also been reported that minor chemical shift differences for the same resonance have been observed in different samples.[6] Systematic temperature dependent studies of Xe spectra in clathrate hydrates are needed to provide unambiguous tests of our predictions in Table VI.

DISCUSSIONS

Monte Carlo averaging results in a different line shape than that which is calculated from the Xe shielding tensor at the center of each type of cage. Unlike Xe in C_{60}, there is some free volume for Xe atoms to explore in each of the cages of clathrate structures I and II. This averaging leads to a Xe tensor that is at higher chemical shift than for a static Xe atom at the center of the cage. For each of the four types of cages, about 20 to 50 ppm deshielding is gained by averaging. Another consequence of the dynamics is to average out local shielding tensor asymmetries. The apparent anisotropy of 9.0 ppm at the center of the 5^{12} cage of structure I is averaged out to 0.7 ppm by Monte Carlo averaging in the same XCAGE. We discovered that the average shielding tensor components in a single XCAGE is not statistically different from the average shielding tensor components obtained in the supercell of 384 cages of type $5^{12}6^2$ in structure I or 128 cages of type 5^{12} in structure II. Local sampling of different proton arrangements is apparently sufficient.

Although the differences in O–O distances found in the 5^{12} cages of type I and type II are very small, the Xe atom is sensitive to these small differences. The shielding response in the 5^{12} cages in type II do reflect the existence of a unique pair of oxygen atoms in the 5^{12} cage of type II, which leads to an axially symmetric Xe tensor with about 20 ppm anisot-

ropy. The small remaining anisotropy from the simulations at 275 K, in cages that should have given rise to isotropic signals at a temperature high enough for molecular reorientation to effectively average out the proton disorder, reflect the inability of simulations of Xe in cages with static configurations to completely represent the dynamically averaged configuration, even when using supercells with 128 and 64 cages, respectively, of type 5^{12} in structure I and $5^{12}6^4$ in structure II. Using an ''averaged'' clathrate structure would of course have led to three identical average tensor components for these cages. For example, to mimic clathrates under fast molecular reorientation, we could have used a static configuration with each proton located at the center of the O–O line. Alternatively, we could have placed twice as many protons in the simulation box, at the positions located by neutron diffraction, and used half the Xe–H shielding function and half the Xe–H potential function in the Monte Carlo simulations. However, neither one of these two possible representations of ''averaged'' cage structures would have resulted in an accurate one-body distribution functions. The probability of finding a Xe atom in a particular location within a cage depends on the instantaneous configuration of oxygen and hydrogen atoms, which would be falsely represented by either one of these simple ''averaged'' representations. For this reason, we choose the more complex representation of the crystal using supercells. Indeed, Table I shows that the residual anisotropy of 0.7 and 1.3 ppm obtained in averaging over a single XCAGE reduces to only 0.1 ppm upon averaging in supercells.

All 5^{12} cages in clathrate hydrates I, II, H, and bromine hydrate have been found in this work to have Xe isotropic chemical shift values in the range 208–233 ppm at 275 K, in good agreement with experiment (range 232–254 ppm at 200–240 K, and at room temperature). The relative magnitudes of the anisotropies of the nonisotropic average tensors are reasonably well reproduced, largest for Xe in the $4^35^66^3$ cage of clathrate hydrate type H, smallest for Xe in the $5^{12}6^2$ cage of type T_B in bromine hydrate. (The smallest anisotropy of the anisotropic tensors was calculated in the $5^{12}6^3$ cage (P) in bromine hydrate, but this has not been observed experimentally.) The Xe chemical shift tensors in the entire range of Xe environments observed in clathrate hydrates, from 80 to 250 ppm are well represented in these calculations. The absolute agreement with the isotropic Xe chemical shifts is reasonably good, except for the Xe chemical shift in the $5^{12}6^4$ cage of structure II which is overestimated by about 20%. The relative positions of the peaks and their individual line shapes are in excellent agreement with the experiments of Ripmeester and co-workers.[5,6,32]

We are unable to have quantitative agreement with some finer details, for example, the relative magnitudes of the anisotropies of Xe in the $5^{12}6^2$ cage in type I and the 5^{12} cage in type II. We find nearly the same value of the span for both whereas the experimental data reveal that Xe in the $5^{12}6^2$ cage has a larger span than does Xe in the 5^{12} cage. On the other hand, we do find excellent predictive capabilities by our methodology overall, when we compare the predicted NMR spectra for Xe in 12 different cages, with spectra that have been observed experimentally for ten of these cage types. Our method provides unequivocal predictions, given the same set of quantum mechanical shielding functions and empirical potential functions, and all results are directly comparable since we do not adjust any parameters to observed NMR spectra. Agreement with experiment can still be improved by improving the Xe–O and Xe–H potential functions used. This may be most important for the largest cages with the largest free volumes for Xe, where changing the potential functions used could lead to significant changes in the Xe one-body distributions that weight the shielding contributions from cage atoms. The dimer tensor model appears to be adequate in representing the quantum mechanical values of Xe shielding tensors. Improvement would require the inclusion of nonadditive terms (three-body and higher) in the fitting of the *ab initio* values.

CONCLUSIONS

We have calculated for the first time, and starting from first principles, the line shapes that are observed in the ^{129}Xe nuclear magnetic resonance spectra of xenon in the cages of clathrate hydrate structures I, II, H, and bromine hydrate. In the dimer tensor model, the shielding response tensor components for a Xe at a specific location in a clathrate cage from quantum mechanical calculations using an extended cage model (XCAGE/PCA) are represented by contributions from parallel and perpendicular tensor components of Xe–O and Xe–H dimers. The shielding tensors reconstructed from the Xe–O and Xe–H parallel and perpendicular shielding functions are employed in canonical Monte Carlo simulations to calculate the Xe shielding tensor component along a particular magnetic field direction. The shielding tensor components weighted according to the probability of finding a crystal fragment oriented along a particular laboratory direction in a polycrystalline sample lead to a predicted line shape.

The line shapes calculated for Xe in the 12 types of cages in clathrate hydrate structures I, II, H, and bromine hydrate using *the same* shielding functions and *the same* potential functions, are in excellent agreement in terms of the existence of anisotropy, the sign of the anisotropy, and the magnitude of the anisotropy, with the line shapes observed experimentally by Ripmeester and co-workers in Xe type I hydrate, in Xe–propane type II hydrate, in Xe type H hydrate, and in bromine hydrate.[5,10,11,32] We have assigned the individual average tensor components to specific axes of the cages or the crystal. While the agreement with the experimental values that can be deduced from the Xe spectra is not excellent in every case, we believe the assignments of relative magnitudes of the components to the specific principal directions are reliable. Such assignments cannot be unequivocally determined from the experimental spectra in many cases.

We have established that the average Xe shielding tensor of a single Xe atom in a cage reflects the symmetry of the cage itself, as canceling contributions of equal magnitude, and opposite signs, are uniformly included in the averaging process through built-in proper statistical sampling. Thus, the Xe NMR line shapes directly provide information about the symmetry of the cage, in the number of unique components,

and in the relative magnitudes of the components parallel and perpendicular to the symmetry axis of the cage itself. Provided that the Xe in the cage is not undergoing fast exchange with other sites within the crystal or in the overhead gas, this knowledge permits the determination of structural information from observations of Xe NMR spectra, which has been the expressed motivation of Ripmeester and coworkers for their beautiful experimental work, since 1981, using the ^{129}Xe nucleus as a general probe of voids.

ACKNOWLEDGMENTS

This research was funded by the National Science Foundation (Grant No. CHE-9979259), for which continued support we are very grateful. We thank Devin Sears for generous assistance in preparing Figs. 8–10.

[1] C. A. Koh, Chem. Soc. Rev. **31**, 157 (2002).
[2] J. L. Bonardet, J. Fraissard, A. Gedeon, and M. A. Springuel-Huet, Catal. Rev. - Sci. Eng. **41**, 115 (1999).
[3] C. I. Ratcliffe, in *Annual Reports on NMR Spectroscopy*, edited by G. A. Webb (Academic, London, 1998), Vol. 36, pp. 123–221.
[4] B. M. Goodson, J. Magn. Reson. **155**, 157 (2002).
[5] J. A. Ripmeester, C. I. Ratcliffe, and J. S. Tse, J. Chem. Soc., Faraday Trans. 1 **84**, 3731 (1988).
[6] J. A. Ripmeester and D. W. Davidson, J. Mol. Struct. **75**, 67 (1981).
[7] D. W. Davidson, Y. P. Handa, and J. A. Ripmeester, J. Phys. Chem. **90**, 6549 (1986).
[8] J. A. Ripmeester, J. Am. Chem. Soc. **104**, 289 (1982).
[9] M. J. Collins, C. I. Ratcliffe, and J. A. Ripmeester, J. Phys. Chem. **94**, 157 (1990).
[10] J. A. Ripmeester and C. I. Ratcliffe, J. Phys. Chem. **94**, 8773 (1990).
[11] I. L. Moudrakovski, C. I. Ratcliffe, and J. A. Ripmeester, J. Am. Chem. Soc. **123**, 2066 (2001).
[12] F. Lee, E. Gabe, J. S. Tse, and J. A. Ripmeester, J. Am. Chem. Soc. **110**, 6014 (1988).
[13] J. A. Ripmeester and C. I. Ratcliffe, J. Phys. Chem. **99**, 619 (1995).
[14] I. L. Moudrakovski, A. Nossov, S. Lang, S. R. Breeze, C. I. Ratcliffe, B. Simard, G. Santyr, and J. A. Ripmeester, Chem. Mater. **12**, 1181 (2000).
[15] I. L. Moudrakovski, C. I. Ratcliffe, and J. A. Ripmeester, Appl. Magn. Reson. **10**, 559 (1996).
[16] C. J. Jameson, D. N. Sears, and A. C. de Dios, J. Chem. Phys. **118**, 2575 (2003).
[17] C. J. Jameson, J. Chem. Phys. **116**, 8912 (2002).
[18] A. K. Jameson, C. J. Jameson, and H. S. Gutowsky, J. Chem. Phys. **53**, 2310 (1970).
[19] C. J. Jameson, A. K. Jameson, and H. Parker, J. Chem. Phys. **70**, 5916 (1979).
[20] C. J. Jameson, A. K. Jameson, and S. Wille, J. Chem. Phys. **74**, 1613 (1981).
[21] C. J. Jameson and A. K. Jameson, J. Chem. Phys. **81**, 1198 (1984).
[22] C. J. Jameson and A. K. Jameson, J. Magn. Reson. **62**, 209 (1985).
[23] C. J. Jameson (unpublished).
[24] D. Stueber and C. J. Jameson, J. Chem. Phys. **120**, 1560 (2004).
[25] G. C. Maitland, M. Rigby, E. B. Smith, and W. A. Wakeham, *Intermolecular Forces, Their Origin and Determination* (Clarendon, Oxford, 1981).
[26] C. J. Jameson, A. K. Jameson, P. Kostikin, and B. I. Baello, J. Chem. Phys. **112**, 323 (2000).
[27] M. P. Allen and D. J. Tildesley, *Computer Simulations of Liquids* (Clarendon, Oxford, 1987).
[28] R. K. McMullan and Å. Kvick, Acta Crystallogr., Sect. B: Struct. Sci. **B46**, 390 (1990).
[29] C. J. Jameson and A. C. de Dios, J. Chem. Phys. **116**, 3805 (2002).
[30] J. A. Ripmeester, J. S. Tse, C. I. Ratcliffe, and B. M. Powell, Nature (London) **325**, 135 (1987).
[31] G. Miehe, T. Vogt, H. Fuess, and U. Mueller, Acta Crystallogr., Sect. B: Struct. Sci. **B49**, 745 (1993).
[32] K. A. Udachin, G. D. Enright, C. I. Ratcliffe, and J. A. Ripmeester, J. Am. Chem. Soc. **119**, 11481 (1997).
[33] A. D. Buckingham and S. M. Malm, Mol. Phys. **22**, 1127 (1971).
[34] T. Ikeda, S. Mae, O. Yamamuro, T. Matsuo, S. Ikeda, and R. M. Ibberson, J. Phys. Chem. A **104**, 10623 (2000).